Analysis on Common Rail diesel engine combustion process by optical diagnostics

S.S. Merola and B.M. Vaglieco
Istituto Motori-CNR , Napoli -Italy

ABSTRACT

This paper reviews a number of recent investigations in Common Rail diesel passenger car engines using examples from relevant research investigations already performed or presently in progress at the Fluid-dynamic, Combustion and Fuel Cell for Propulsion Division of Istituto Motori using optical diagnostic techniques. The paper discusses diesel combustion fundamental processes in terms of the in-cylinder flow, sprays, combustion and emissions. Emphasis is placed on combustion systems and spectroscopy techniques able to analyse the processes that control engine-out emissions and fuel consumption.

Key words: diesel engine, common rail, optical diagnostics, combustion process.

INTRODUCTION

As predicted in the past, the diesel engine penetration has largely passed the 40% share of the European market of passenger cars and it is easy to predict a further growth in the next years up to around 50 %.

This great success is certainly due to the late 90s' availability of technology breakthrough for the fuel delivery system, as Common Rail (CR) and unit injector, which have led to enhance the direct diesel engine potential in term of fuel economy and fun to drive granting a superior control of emission, noise vibration and hardness, the traditional weak points of the solution. [1, 2, 3]

However, the diesel engine challenge continues in the next future with the mandatory step of the gasoline convergence on exhaust emission.

Therefore a new great research effort is requested both industries and research laboratories to study fundamental process involved in diesel engines in order to define possible technical trends and strategic scenario toward zero emission level. [4]

Modern diesel engines are improved in terms of performances and emissions thanks to the fuel injection through electronically controlled high-pressure Common Rail (CR) systems. The recent multiple injection strategy has been a valid help to improve the combustion quality reducing the soot formed during the first stage and stimulate the soot oxidation in the last stage of the combustion by post injection pulses. [5, 6, 7]

For this target, the study of physical and chemical processes involved in CR diesel engine is necessary by basic and advanced experiments. Because of the difficulty in study of physical and chemical processes involved optical diagnostic techniques are particularly useful. In these last years, the availability of transparent engines, comparable with production engines, have allowed valuable information until now about fuel spray distribution and evaporation, mixture preparation, auto-ignition, spatial distribution of key transient species, and, finally, pollutant formation. [8, 9]

In this paper, CR diesel processes from fuel injection to exhaust phase were analysed by combined optical measurements. They were based on 2D digital imaging and spectroscopic technique such as Ultraviolet (UV) to visible scattering extinction and absorption and flame emission measurements.

These investigations were carried out on three diesel research systems equipped with CR injection system: a 1.9 litre, 4 cylinder, 16 valves, direct-injection diesel engine equipped with catalysed DPF (known as CSF, Catalysed Soot Filter), an optical d.i. equipped with the multi-cylinder head and multi injection system, and finally a diesel system developed "ad hoc" by modifying a real engine in order to realize an external accessible chamber equipped with a single-hole injector located centrally on the top of the external chamber.

All diesel systems were equipped with a programmable electronic controlled Common Rail system to manage the injection pulses and the dwell time.

DIESEL COMBUSTION STUDY BY OPTICAL DIAGNOSTICS

The optics has always played an important role in the measurement and understanding of processes involved in internal combustion engines during these thirty years. In particular, being the diesel combustion a two-phase, turbulent mixing-controlled process that includes short time scale phenomena such as turbulence production and dissipation, spray break-up and evaporation, and pollutants formation [10] it is appropriate to make investigation by optical diagnostic techniques that are not intrusive and have high temporal and spatial resolution.

First of all high speed direct, backlight and Schlieren cinematography were applied to study spray atomisation, fuel penetration and evaporation phenomena [8]. Then laser sources and new detection systems have permitted to set new 2-D laser sheet imaging diagnostics [11].

The spatial distribution of liquid and vapour of fuel was made inside optical accessible diesel system both by simultaneous use of laser induced Rayleigh and Mie-scattering imaging and EXCIPLEX technique, based on a fluorescence system [8, 11]. A different technique, based on the principle of absorption of ultraviolet laser light by fuel vapour and the scattering of visible laser light by fuel, seemed to give good results because it measures simultaneous the concentrations of vapour and liquid in an evaporating diesel spray [12, 13]. Being an absorption technique, its drawback is the integration across the entire width of spray.

Experimental analysis of intermediate steps of ignition and onset of soot formation combustion was generally restricted to measurements of ignition delay and high-speed photography, doping the fuel with copper to create a more luminous emission before the soot formation occurs [8]. These techniques lacked of spatial and time resolution and have been overcame partly by imaging the natural chemiluminescence using calibrated intensified video camera. [14, 15, 16]

Luminosity imaging and simultaneous planar imaging of laser–induced incandescence and elastic scattering have contributed to detect the onset of soot during the range of time in which a solid particle is formed from fuel molecules. [15, 16, 17, 18]

Light extinction, Rayleigh and Mie scattering, laser induced incandescence (LII) and laser induced fluorescence (LIF) have allowed to follow the soot formation and oxidation process in terms of soot particle size and number density, temperature and some species concentration. [14-18]

Recently, simultaneous multi-wavelength scattering extinction and absorption measurements, from UV to visible have shown a sufficient sensitivity to yield useful information on sizing, morphological characterization and the particulate nature and NO in the cylinder and in undiluted exhaust. [8, 19, 20, 21]

EXPERIMENT DESCRIPTION

ENGINES

Optical single cylinder diesel engine

The optical access engine used during experiments was a single cylinder, direct injection, and four-stroke diesel engine, with a multi-valves production head of JTD 1.9 litre. The engine had a bore of 85 mm and a stroke of 92 mm. An air compressor supplied pressurized intake air that was dehumidified, highly filtered and heated. The head had four valves per cylinder that were equipped with hydraulic tappets and moved by a double overhead camshaft. A rotational motion of the air, entering in the cylinder, was obtained by means of intake port with helical shape.

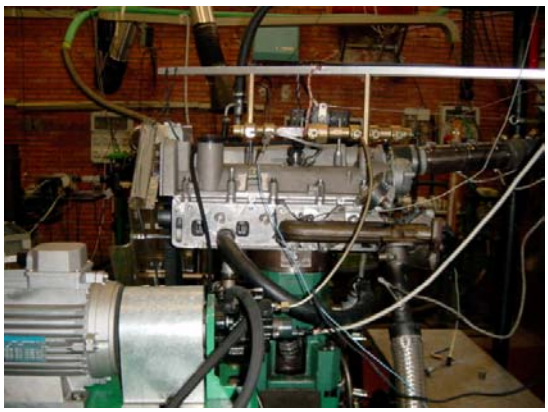

(a)

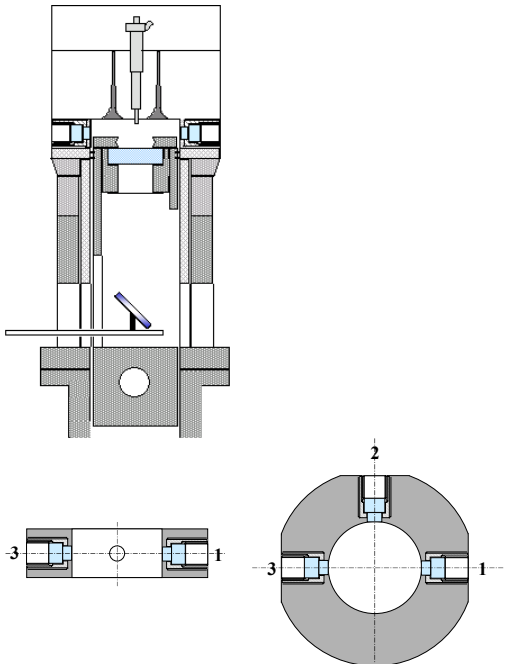

(b)

Figure 1. Optical accessible engine layout with (a) a photo of engine head and (b) detailed sketch of the steel crown.

The production head was designed for the four-cylinder engine thus it was necessary modifying the head for the single cylinder research engine. Also a water-cooled quartz piezoelectric pressure transducer was set in the glow plug seat. Particular attention to the water-cooling and lubricating oil head conducts was devoted. The design of the engine utilized a classic extended piston with piston crown window (diameter of 34mm).

A steel crown was placed between the cylinder head and cylinder block. Inside this, heated liquid flowed in order to keep a homogenous temperature for the three different blocks. Three windows (diameter of 15.8 mm) were made on the steel crown to provide orthogonal and longitudinal optical accesses.

Engine type	4-stroke single cylinder
Bore	8.5 cm
Stroke	9.2 cm
Swept volume	522 cm^3
Combustion chamber volume	21 cm^3
Volumetric compression ratio	17.7:1

Table 1. Optical Single Cylinder Engine specifications

The piston crown window provided a full view of the combustion bowl. Inside the extended piston, it was possible to arrange an appropriate 45° UV-visible mirror that permitted to investigate the combustion process. The combustion bowl had a toroidal shape. Table 1 reports specification of the optical–access engine. More details and specifications on engine are reported in [15, 16].
The injector was located centrally and has the same cylinder axis, it was equipped with a single guide microsac nozzle, with 6-holes (diameter of 0.145 mm). The nominal angle of the fuel jet axis was 16° downward from horizontal and the rated flow corresponded to 400 cm^3/30 s @ 100 bar [22].

External chamber diesel system

A single cylinder, air-cooled, naturally aspirated, four-stroke diesel engine having a displacement of 750 cm^3 (a bore of 100 mm and a stroke of 95 mm) was modified to provide an external combustion chamber on the cylinder head connected to the main chamber by a tangential duct (Figure 2). In order to have a suitable compression ratio and obtain an externally accessible combustion chamber, the standard piston, having a toroidal bowl, was replaced with a flat one. The compression ratio was set to 22.3:1 to compensate for the increased heat losses due to the external chamber. A single guide KS microsac nozzle single-hole (diameter of 0.145 mm) was located centrally on the top of the external chamber. the rated flow corresponded to 67 cm^3/30 s @ 100 bar [22].

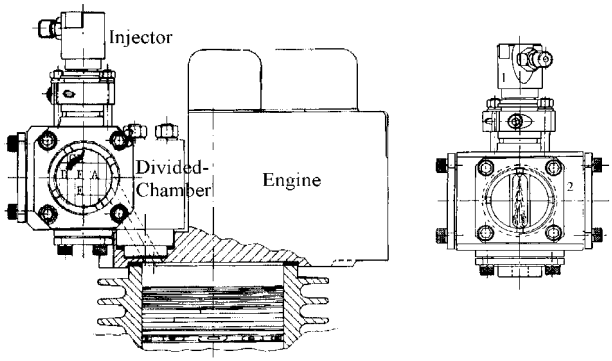

Figure 2. Frontal and lateral view of the engine 1) injector and 2) lateral view.

The external chamber has the same piston-bowl volume as the unmodified engine (21.3 cm^3) and has cylindrical geometry (radius=15 mm and height = 28.0 mm). Table 2 reports the engine specifications.
Three wide optical accesses were made: two circular windows in the longitudinal direction (diameter = 30 mm) and an elliptical window in the orthogonal one (10 x 30 mm).

Modified engine type	Diesel-4 stroke
Bore	10.0 cm
Stroke	9.5 cm
Displacement	750 cm3
Connecting rod length	17 cm
Divided-chamber volume	21.3 cm3
Connecting duct diameter	0.8 cm
Clearance height at TDC	0.15 cm
Volumetric compression ratio	22.3:1

Table 2. External Accessible Chamber Engine specifications

A strong air vortex was generated during the compression stroke because of the pressure difference between the main chamber and the external one connected by tangential duct. The engine could be operated continuously for several minutes, limited only by the rise in the cylinder head temperature. It took a couple of hours of accumulated engine running before the windows must be taken off and cleaned because they were shielded from the fuel sprays by the rotating airflow. More details and specifications on engine are reported in [18, 19].

Multi cylinder engine

A turbo charging four-stroke CR diesel engine, with four in-line cylinders 16 valves, a displacement of 1.9 litre and a compression ratio of 17.5:1, representative of light-duty class, was used. Injectors have 6-holes (diameter of 0.155 mm) and are single guide KS microsac [20, 21].

The engine exhaust was equipped with DPF. The DPF was a 5.66” x 6” silicon carbide (Ibiden) coated with CeO_2 (400 g/ ft^3) and Pt (75 g/ ft^3) [23]. The catalyst

coated directly the ceramic walls of the filter material to achieve spontaneous regeneration of collected PM at lower temperature with respect to non-catalysed DPF.

Engine type	1910 JTD
Cylinder	4 cyl. in-line
Bore	82 mm
Stroke	90.4 mm
Displacement	1910 cm^3
Volumetric compression ratio	18.45

Table 3. Multi Cylinder Engine specifications

Common Rail injection system.

All engines tested were equipped with multi-injection Common Rail system.

The CR system used in these engines consisted of a radial three-piston high-pressure pump, that supplied a Common Rail from which the fuel goes to injectors, and a programmable electronic control unit that allowed to control the rail pressure and injections. This generation CR injection system permits to reach the maximum injection pressure of 1500 bar. A fully flexible Programmable Electronic Controlled Unit (PECU) led it. In particular the PECU controlled the number of injections (till 5) for each cycle, the start and the duration of injection as well as the dwell time between the consecutive injections by means of the current that flow inside the solenoid of the injector. [4]

DATA ACQUISITION AND OPTICAL SETUP

All the engines tested were motored and the speed controlled by 100 and 50 kW dynamometer, respectively.

All experiments were made measuring the combustion pressure both in the external and main chambers by water-cooled quartz piezoelectric pressure transducers A Hall effect sensor detected the solenoid current and a reluctance sensor recorded the injector needle lift. Finally, a piezoelectric pressure transducer was located in the injection line between the rail and the injector to measure the injection pressure.

Cylinder pressure, needle lift and injection pressure were digitised and recorded at 0.1 crank angle degree increments and ensemble-averaged over 16 consecutive combustion cycles

In order to relate the physical and chemical processes inside the combustion chamber to exhaust emission particulate and gas emission were sampled. Smoke was measured by opacimeter and gas emission in terms of HC, CO, CO_2 and O_2 was measured by infrared analysers and NO_x by chemiluminescence analyser. TEM observations were carried out on particulate collected in-situ by TEM grid. In all experiments, synchronisation between different engine phase, detection system and light sources was controlled by the unit delay with the signal coming from the engine shaft encoder.

Single cylinder optical apparatus

The set up shown in Figure 3 was used to characterise processes in single cylinder optical engine. In particular, the temporal and spatial evolution of the diesel spray were followed analysing the images obtained with a gated intensified CCD lighting the spray with a high luminous CW Halogen and pulsed UV Xenon lamp.

On the other hand, combustion phase was characterized by spectroscopic methods and by imaging the natural chemiluminescence and flame luminosity. Flame signals were collected and focused by a 150 mm focal lens on the entrance slit of a spectrograph (f/3.8 with 150 mm focal length). The flame emission was detected by a gated intensified CCD (512 x 512 pixels) with every pixel of 20x20 μm^2 using an intensifier with gate duration of few nanoseconds (ns) in order to have a good accuracy in the timing of the onset of the combustion and pollutant formation process. The spectral image formed on the spectrograph exit plane was matched with ICCD camera. Emission measurements were corrected by dark noise and spectral response.

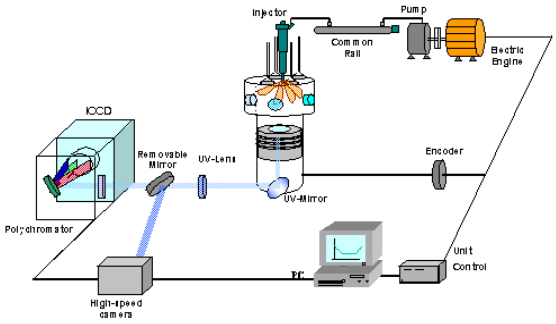

Figure 3. Experimental apparatus for optical single cylinder engine

Radicals and flame imaging were acquired with the same ICCD equipped with a UV Nikon 78 mm f/3.8-2.2 lens and UV and visible narrow band pass filters chosen at characteristic wavelength of OH (λ=309 nm) and CH (λ=431 nm) [24].

Although each spectrum or image had an effective exposure time of few μs, only one could be acquired in a given cycle due to speed limitations of acquisition system. Spectra and images were acquired in sets of 10 or 20, from 10 or 20 separate cycles. Each spectrum and/or image reported was not the average. They were subjectively selected as being representatives of their respective set. More details and specifications on optical apparatus are reported in ref. [19].

External chamber diesel system optical apparatus

Absorption, extinction and scattering measurements were carried out in the wavelength range 190 - 550 nm with a light source exploiting the emitting plasma kernel of an optical breakdown. It was obtained by tightly focusing in air a ns Q-switched laser pulse [25]

Flame emission, scattering and extinction signals were collected and focused by a lens (f = 200 mm) on the input slit of luminous spectrograph (f/3.8 with 270 mm focal length). All signals were detected by the same gated intensified CCD previously described (Fig. 4). Scattering signals were detected at an angle θ=90°and calibrated using CO_2 as reference gas. CO_2 has a scattering cross section higher than air of about an order of magnitude at ambient pressure and temperature and is not flammable in presence of spark. Extinction and absorption measurements did not need of signal calibration. All measurements were evaluated on an optical path of 2.8 cm.

To minimise the statistical uncertainty of the results, the extinction, scattering and flame intensity measurements are detected in sets of 30, from 30 separate combustion cycles. In particular, getting average measurements on 30 combustion cycles allows minimising the effect of cycle-to-cycle engine variations. As a consequence, the collected spectra show a great repeatability. Each measurement presented is subjectively selected as being representative of its respective set.

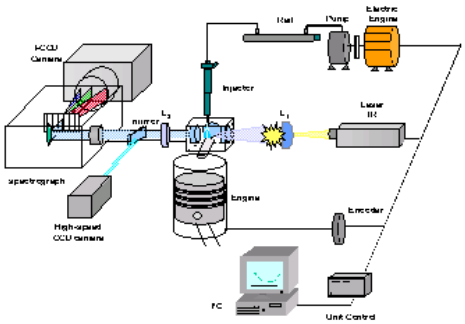

Figure 4. Experimental apparatus for external chamber engine.

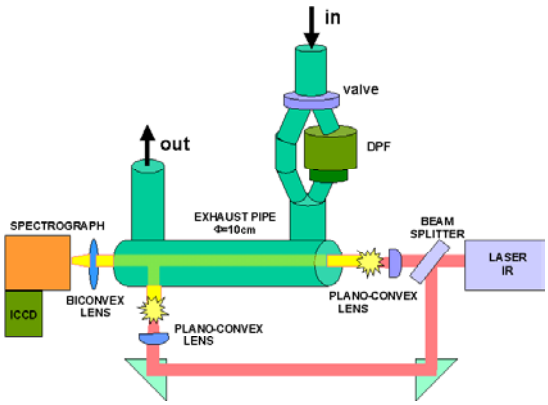

Figure 5. Optical apparatus used for multi cylinder exhaust measurements.

Exhaust optical apparatus

The schematic picture of optical experimental apparatus used to characterize the exhaust is shown in Figure 5. The optical test section was placed at 100 cm, downstream engine exhaust valves. This distance was chosen as a good compromise to reduce the speed of exhaust flow and to avoid coagulation effects caused by the increase of the permanence time in the test section. The exhaust temperature was monitored in real time by several thermocouples set along the pipe. A still plug valve permitted to the gas exhaust to flow or not in the optical measurement volume.

Absorption, extinction and scattering measurements were carried out using the same broadband-pulsed light source of optical apparatus for external chamber engine. [25]
Extinction and scattering signals were collected and focused with an UV-grade fused silica biconvex lens (15 cm focus length) on the entrance slit (200 μm) of a spectrograph (f/4 with 15 cm focal length). The spectral image formed on the spectrograph exit plane was detected with a gated ICCD camera. Measurements were performed in the spectral range UV-visible from 190 to 600 nm.

In order to reduce the statistical uncertain, the scattering and extinction measurements were carried out over 100 consecutive exhaust cycles, using laser shots at a frequency repetition of 20 Hz.

MATHEMATICAL FORMULATION

EXTINCTION-ABSORPTION TECHNIQUE FOR VAPOR-LIQUID PHASE

UV-visible extinction-absorption measurements allowed to characterize the vapour and liquid phase of the diesel fuel because typical absorption bands of fuel compounds are present in this range. The concentration of both phases can be obtained using the principle of absorption of the ultraviolet light by fuel vapour and the scattering of the light in the visible range by the liquid fuel droplet [12,13]. In particular, as observed in previous investigation [26, 27], the liquid phase of the diesel fuel spray is characterized by a broad spectrum with high intensity in the UV and a flat profile in visible range while the vapour phase of spray shows a peak only in the UV.

Considering a polychromatic light beam with intensity I_0, passing through a bi-phase spray, an attenuated and transmitted light intensity I_t can be obtained according to the Lambert – Beer's law:

$$\frac{I_t}{I_0} = \exp\left(-K_{ext} \cdot L\right) \qquad (1)$$

Where L is the optical path length and K_{ext} is the extinction coefficient.

The visible light is not absorbed by both liquid and vapour phases and it is attenuated only by the scattering caused by droplets. Therefore, the transmissivity of the visible light by the fuel spray is equal to the transmissivity due only to the scattering caused by liquid droplets, as shown by the following equation:

Visible

$$\log\left(\frac{I_0}{I_t}\right)_{Vis} = \log\left(\frac{I_0}{I_t}\right)_{L,sca} \qquad (2)$$

The ultraviolet light, which is absorbed by both liquid and vapour phases, is attenuated due to the absorption caused by the vapour, to the scattering caused by liquid droplets and to the absorption of liquid droplets and then:

UV

$$\log\left(\frac{I_0}{I_t}\right)_{UV} = \log\left(\frac{I_0}{I_t}\right)_{V,abs} + \log\left(\frac{I_0}{I_t}\right)_{L,sca} + \log\left(\frac{I_0}{I_t}\right)_{L,abs} \qquad (3)$$

In the equation (3) the last two terms are much lower than the first one, so the vapour transmissivity can be written as:

$$\log\left(\frac{I_0}{I_t}\right)_{V,abs} \propto \log\left(\frac{I_0}{I_t}\right)_{UV} - \log\left(\frac{I_0}{I_t}\right)_{Vis} \qquad (4)$$

According to relation (2) and (4), it is possible to retrieve a qualitative temporal and spatial distribution of vapour and liquid by evaluating the ultraviolet and visible transmissivity.

EXTINCTION-SCATTERING TECHNIQUE FOR SIZE OF FUEL DROPLET AND SOOT

The measured scattering signals obtained from a probe volume at fixed scattering angle θ at a wavelength λ can be expressed, through a calibration procedure, in terms of the angular scattering coefficient Q(θ). This quantity is defined as the energy scattered from a unit volume, per unit solid angle, for an incident beam of unit intensity [8, 28]. When the incident light comes from an unpolarised source, as in this work, the measured scattering coefficient $Q_{unp}(\theta)$ can be explained by the relation:

$$Q_{unp}(\theta) = N\, C_{scat}(D, n, k, \theta, \lambda) \qquad (5)$$

The extinction is the attenuation of an electromagnetic wave by scattering and absorption as it traverses a particulate medium, and it is defined as:

$$K_{ext} = N\, C_{ext}(D, n, k, \lambda) \qquad (6)$$

where N is the number density of the particles in the probe volume, D the diameter, n and k the real and imaginary part of refractive index, respectively. C_{scat} and C_{ext} are the angular cross section for scattering and the total cross section for extinction, respectively

Using the hypothesis that the medium is made of homogeneous spheres of small diameter D, as compared to the wavelength λ of radiation, the spectral scattering coefficients allowed evaluating a medium value of the fuel droplets. The numerical procedure used to retrieve the droplet size was based on the minimization of the difference between the experimental and theoretical Mie scattering spectrum, changing the droplet diameter, known the fuel refractive index.

The Lorenz-Mie theory, converges to the Rayleigh approximation, in the case of small particle ($D<<\lambda$), the Rayleigh approximation can be considered and extinction and scattering coefficients can be written as:

$$K_{ext} = -Nx_2^3\, Im\left(\frac{m^2-1}{m^2+2}\right)\frac{\lambda^2}{4\pi} \qquad (7)$$

$$Q_{ump} = Nx_1^6\left|\frac{m^2-1}{m^2+2}\right|^2 \frac{1+\cos^2\vartheta}{2}\frac{\lambda^2}{4\pi^2} \qquad (8)$$

where $x_1=\pi D_{scat}/\lambda$, $x_2=\pi D_{ext}/\lambda$ and $m=n+ik$ in the case of a monodisperse size distribution with $D_{scatt}=D_{ext}=D$.

In the case of a monodisperse system, the soot particle volume fraction defined as $f_v=N(\pi D^3/6)$ can be evaluated by extinction coefficient, according to the relation (7) as:

$$f_v = \frac{K_{ext}\lambda}{6\pi\left|\mathrm{Im}\left(\frac{m^2-1}{m^2+2}\right)\right|} \qquad (9)$$

Soot particle diameter can be evaluated combining scattering and extinction coefficient, according to relations (7) and (8), known the soot refractive index [29].

In order to evaluate the particle number size distribution, a numerical procedure for retrieving the optical data was used. The inversion procedure was based on the minimisation of the difference between

experimental and theoretical Lorenz-Mie scattering spectrum, known the soot refractive index. The optimising parameter was the mean diameter of a lognormal size distribution [20, 21].

ABSORPTION TECHNIQUE FOR NOX AND OH CONCENTRATION

As is well known in the literature, absorption spectra can be obtained directly from transmission data following Lambert-Beer's law.
The absorption coefficient can be written as:

$$K_{abs} = \sum_i N_i \sigma_{abs}^i \qquad (10)$$

where N_i and σ^i_{abs} are the number concentration and absorption cross section of i^{th} compound, respectively.
It is possible to determine the number concentration known the cross section of molecule detected considering the experiment pressure and temperature. NOx and OH have typical well-resolved absorption bands in the ultraviolet and visible. In particular, OH shows absorption cross section at 309 nm [30], NO has four bands in the spectral range from 190 to 240 nm and NO_2 can be identified by two broad bands centred at 205 nm and 400 nm, respectively. [31]

MIXTURE FORMATION

The mixture formation and first stage of combustion, occurring in diesel engine, are some of the most complex phenomena currently under study because of the increasing interest on new high pressure injection system, like common rail. The analysis of these concurrent processes involved during the ignition delay is complicated by both physical phenomena due to the mixture formation and development of chemical reactions of multicomponent fuels.

The divided chamber system with its three optical accesses allowed to study the single jet at high injection pressure in terms of liquid-vapour distribution, droplets size and penetration. Moreover the single hole jet was compared with multi-hole spray evolution of the optical cylinder d.i. engine. Both systems operated at temperature and pressure of real direct injection engines as reported in Figg. 6 and 9. The investigation was carried out from the start of injection to the end of combustion by spectral measurements from UV to visible using extinction and emissivity and digital imaging.

The mechanism air-fuel interaction and the spatial location of start of combustion were investigated following the progress of fuel injection, vaporization, autoignition and combustion.

Figure 7 reports the digital image sequences carried out from the start of injection to the luminous combustion for engine operating with speed of 1000 rpm, injection pressure of 800 bar and pre and main injections (Fig. 6).

Although the electrical start of pre injection was at 13 CAD BTDC (Fig. 6), the fuel spray was not visible before 11 CAD BTDC (Fig. 7). This shift was due to mechanical delay of the injector.

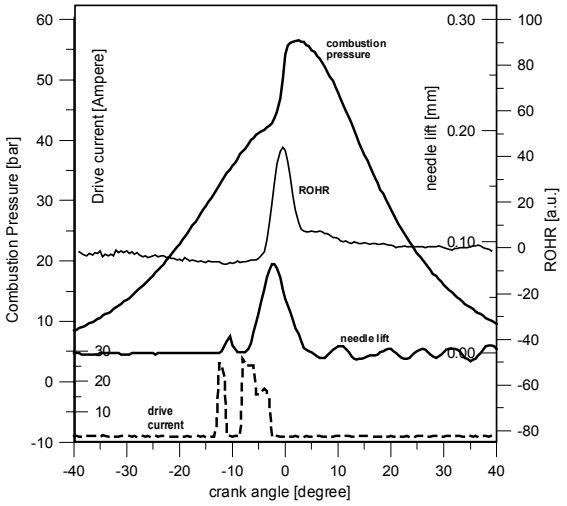

Figure 6. History of the combustion pressure, rate of heat release, driven injector current and needle lift at 1000 rpm and 800 bar detected in the external chamber diesel system.

A good jet atomisation, due to the CR high fuel injection pressure and small injector hole diameter, was observed. During the fuel injection phase, the jet met the swirling air charge and was lightly distorted, due to the high injection pressure, also at low engine speed.

In 1 CAD, the pre spray vaporized rapidly and disappeared before the start of main injection (Fig. 7). However, due to the low local temperature and pressure, the visible combustion did not appear. During the main injection, the liquid jet penetrated almost linearly reaching the maximum length in approximately 3 CAD.

The strong aerodynamic resistance broke up the fuel drops and reduced their size. As injection proceeded, the fuel vaporization took place and the liquid spray became thin and the impingement of the wall was avoided.

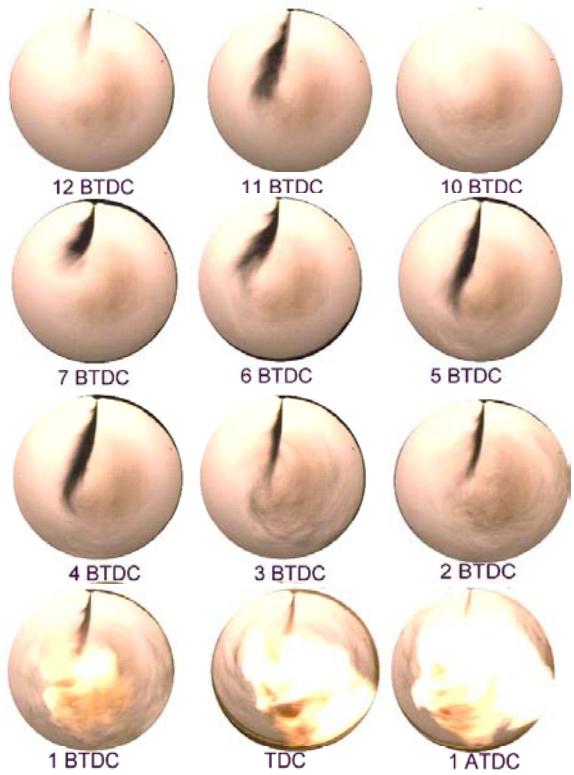

Figure 7. Digital image sequence of spray of single hole injector for engine operating conditions of Fig. 6.

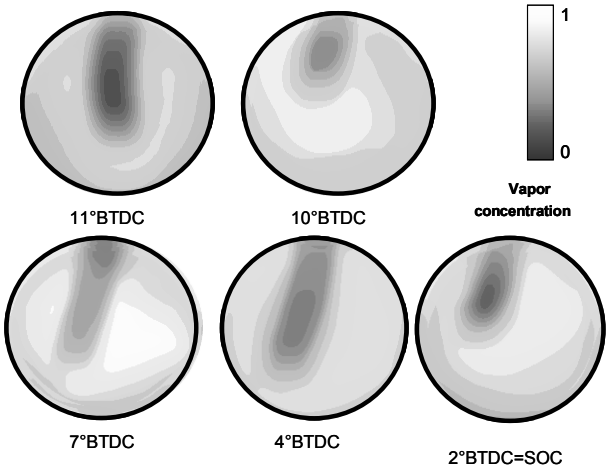

Figure 8. Vapor distribution at different crank angle during the pre and main injections of Fig.6.

The vapour evolution in the chamber was obtained by the UV-visible extinction measurements, according to the procedure explained in the paragraph of mathematical formulation. Some illustrative temporal and spatial distributions of vapour are reported in Figure 8. The vapour spreads around the fuel jet and its concentration evolves from the walls towards the middle of chamber both during the pre and main injection.

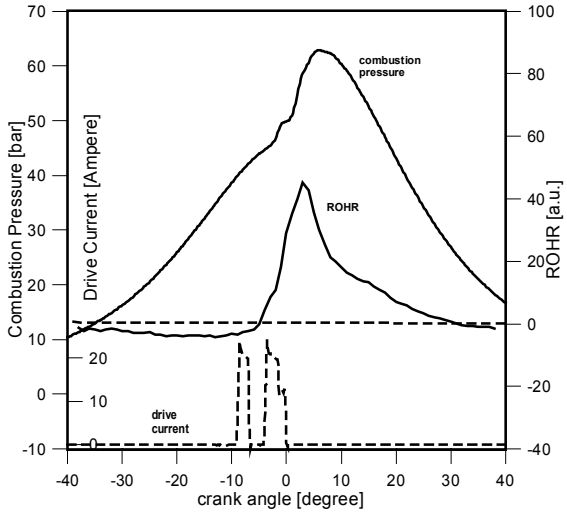

Figure 9. History of the combustion pressure, rate of heat release and driven injector current at 1000 rpm and 800 bar detected in the optical single cylinder d.i. diesel engine.

In Figure 9 the history of the combustion pressure, rate of heat release and driven injector current detected in single cylinder optical engine are reported. Figure 10 shows a part of the injection and combustion sequences of pre and main injections by piston crown window. The shift due to mechanical delay of the injector is observed in multijet case too.

The pre injection is almost symmetrical; the tip of the spray is not deflected by the swirl that is lower than engine tested before. All jets show a dense liquid core that does not impinge on the bottom of the combustion bowl and reaches the maximum penetration in less than 1 CAD. The pre injection can be considered finished at 5 CAD BTDC. It is possible to observe that fuel jet is well atomised on the tip and furthermore the shape and penetration mode of both injections pre and main are similar. The droplets of pre-injection do not ignite immediately, it takes an ignition delay of 4 CAD before that the first start of combustion is observed by in-cylinder pressure signal analysis (Fig. 8).

We can conclude that air-fuel mixing in the two combustion systems (Figures 7 and 9), until to the first luminous flame, does not show substantially differences. These results demonstrate that high injection pressure allows to overcome the swirl influence. It is known that, because of the large pressure difference across the injector nozzle, the liquid fuel enters the chamber at high velocity to atomise into large number of droplets of various sizes and velocities [8, 26, 32]. In high injection pressure system it was observed that the mass of air within the spray increases its width but the spray results less dependent on the level of swirl and turbulence of the fluid flow present in the chamber [10, 33]. Thus the experimental data obtained in external optical accessible chamber referred to the single jet become particular useful to spray investigations.

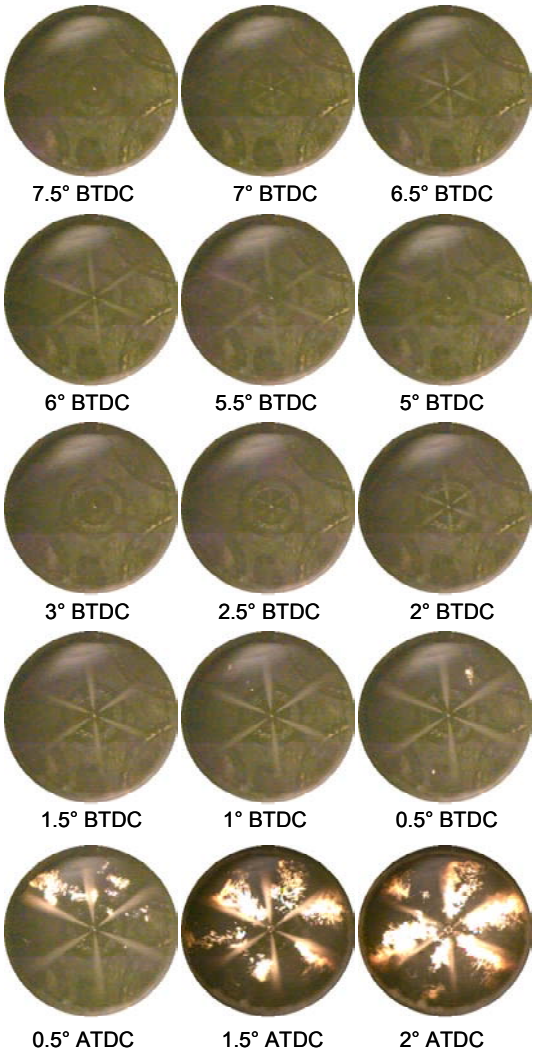

Figure 10. Digital image sequence of spray of six holes injector for engine operating conditions of Fig. 9.

Detailed analysis of fuel size droplet was made during main injection phase, by multiwavelength Mie scattering. Around the fuel jet, scattering measurement show spectral features typical of fuel droplets allowing to evaluate a medium value less than 0.7 μm (Figure 11). Rising to the fuel jet, it is not possible to evaluate the droplet size, due to the fuel liquid film too dense.

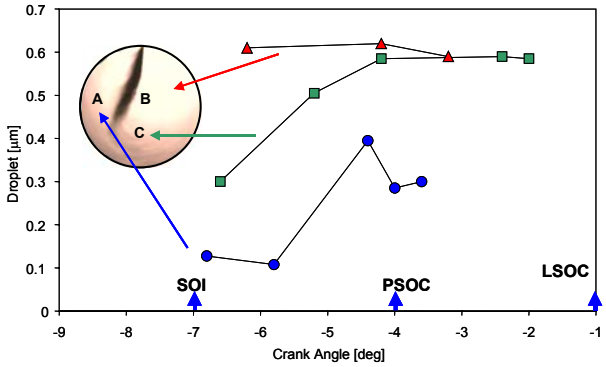

Figure 11. Droplet size evaluated during main injection phase for the engine condition of Fig. 6.

AUTOIGNITION

UV-visible flame intensity measurements have provided an alternative method to determine the occurrence of auto-ignition because they offer the great advantages of high temporal resolution and accurate spatial information and species too. The results have to be considered as the result of integration along the line of sight, which is an intrinsic feature of the measurement technique [8].

Autoignition point is commonly defined as the crank angle when the apparent heat release shows a minimum: this point indicates that the energy release due to combustion exothermic reactions begins to exceed the energy losses due to the evaporative process of fuel. This time generally coincides with the PSOC, identified by the minimum in the first derivative of pressure with respect to time. The ignition point determined applying these considerations can be affected by great uncertainties or errors and sometimes is hard to identify [10].

It is found that the first stage of combustion is spectrally characterised by a weak flame emission, detected mainly in the near ultraviolet range, attributed to natural chemiluminescence.

Chemiluminescence arises from the emission of combustion radicals, typically OH, CH and HCO, due to exothermic chemical reactions occurring during thermal decomposition of the hydrocarbon molecules preceding ignition. This assumption is contrast with those of other papers, analysing diesel combustion engine process with low premixed combustion [14].

The first radical species resolvable by optical signal was observed at PSOC in the external combustion system and was identified as OH. OH distribution at selected crank angle is shown in Fig. 12.

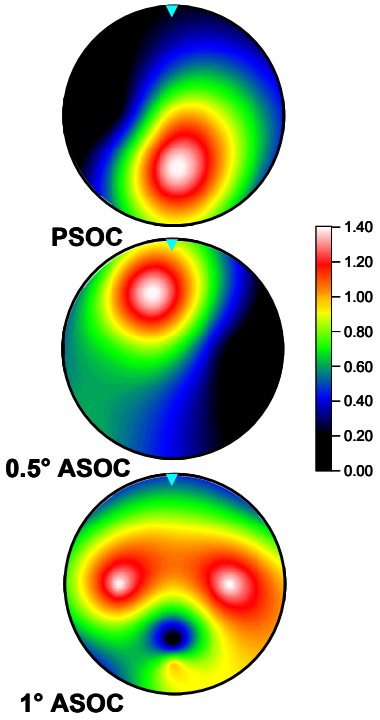

Figure 12. OH distribution evaluated at autoignition during main injection phase for the engine condition of Fig. 6.

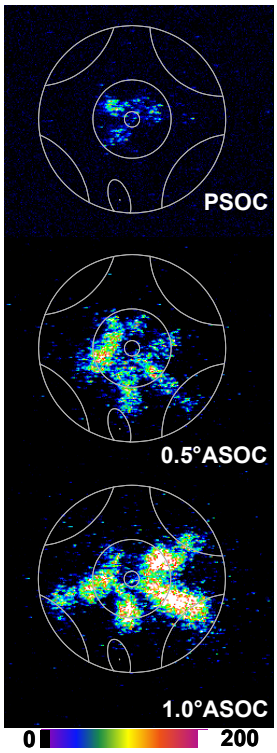

Figure 13. OH distribution evaluated at autoignition during main injection phase for the engine condition of Fig. 9.

At PSOC, the OH detection is indicative of an intense energetic chemical activity, closely marking the occurrence of heat release due to combustion. This is found far from the tip of the liquid, in a region characterised by a large amount of fuel in the vapour phase well mixed with the air entrained in the spray, primarily around the jet and then it proceeded toward the injector location [33].

The phenomenon is fast, because the effect of swirl is highly prevailing and moves the flame involving the whole chamber volume.

Analogous behaviour was observed in Fig. 13. OH signals are higher in the locations placed between two fuel jets and near exhaust valves, where the temperature is higher with respect to the remains of the chamber. OH evolves following the fuel jet traces. The multijets OH signals are lower than single jet. This result is in part due to the different local air-fuel ratio, induced by turbulence of external chamber and in part due to the different optical field of view of the two engines.

COMBUSTION

Many papers have been published to demonstrate the potential of new generation CR system in diesel engines in which the in-cylinder control of pollutant formation has been recognized to be fundamental in reducing engine-out emissions. It is possible to split injection in many steps (1 to 5) to properly control air-fuel distribution and heat release rate. Currently, the multiple injections are not limited to two consecutive injections (pilot + main) and are effective in reducing NOx and soot thanks to the high flexibility to manage simultaneously the number of consecutive injections, the balance of fuel amount per each injection as well as the reduction of the dwell time between consecutive injections. [3-5]

In Figure 14 the flame evolution of pre, main and after injection strategy (Pre+M+A) is reported. It is comparable to Pre+M previously reported (Fig. 10) because engine operated at same engine speed and with the same total fuel amount. For these reasons, same trends and spatial distributions of radicals were observed at the autoignition and during combustion phases. This occurred because the reduction of 10% fuel amount did not induce great change in the evolution of combustion process or in the kind of radical species.

By analysis of UV and visible flame emission reported in Figures 14 and 15, the first optical evidence of after injection was around 13.5 CAD ATDC. Jets penetrated quickly in the high temperature and high-pressure environment of the chamber and thus the ignition delay was particularly short (less than 1 CAD). This time was the start of the post combustion. This had a less intense premixed phase and comparable diffusive phase with respect to main combustion.

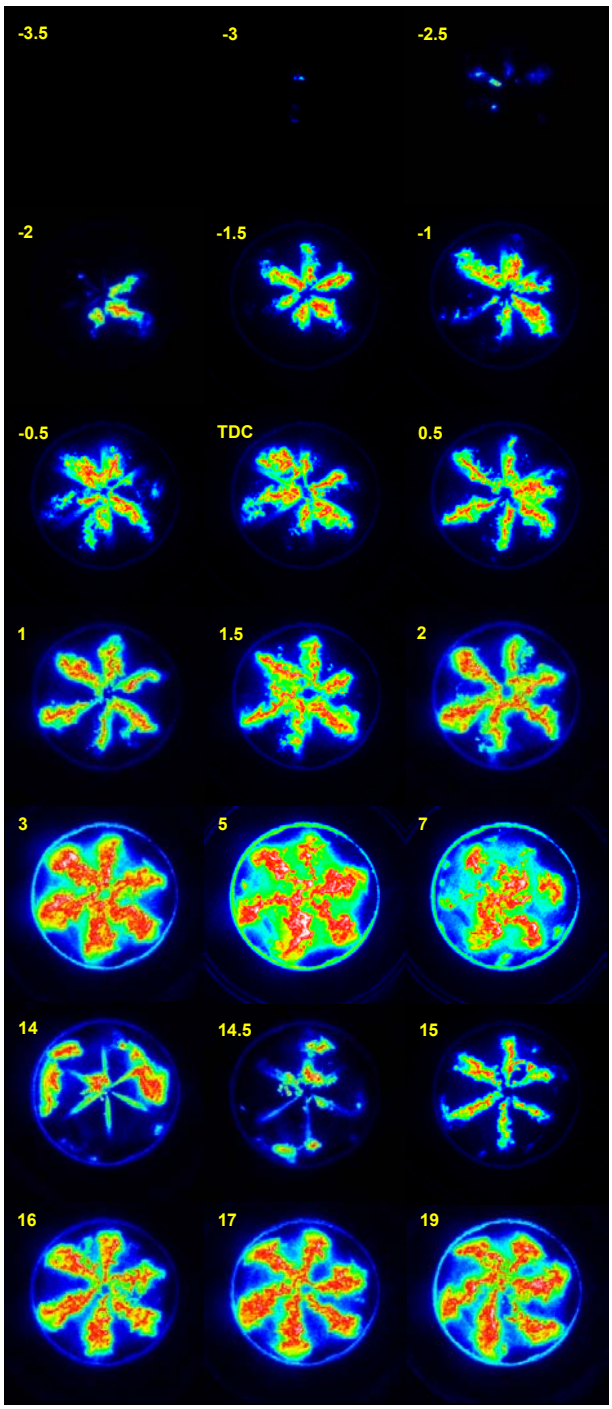

Figure 14. UV-visible flame evolution measured at selected crank angles during Pre+M+A injection strategy.

After the autoignition phase of post injection and until 15 CAD ATDC a fast reduction of OH radicals was observed (Fig.15). OH radicals produced by exothermic reactions of post injection combustion spread in the chamber during the oxidation of soot produced by the main injection combustion. OH contributed to the burning of soot present in the chamber and in particular that near the wall of the chamber (Fig. 15).

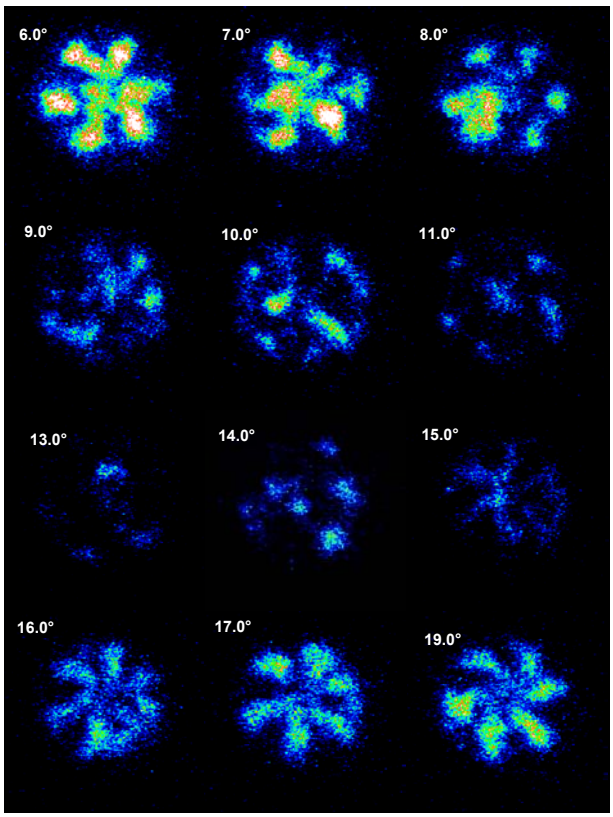

Figure 15. UV emission measured at 309nm for selected crank angles during Pre+M+A injection strategy.

Since 15 CAD ATDC, the post injection was end and visible flame evolved in the chamber along the direction of the jets. This symmetry of the flame distribution still after the end of injection was due to the gradient of air/fuel ratio created by the post injection. The highest intensity of visible emission was around 17 CAD ATDC; on the other hand UV emission increased until 18 CAD ATDC. At this time soot oxidation occurred. Also in this phase the visible flame appeared well confined along the jet direction, until 21 CAD ATDC. At this time flame did not spread in the chamber homogenously for around 7 CAD, coming back close to injector region. OH radicals showed analogous time evolution; on the other hand in the last combustion phase the OH seemed distributed just around soot.

Finally, the persistence and high concentration of OH radicals in the after injection combustion induced a good burning of soot but promoted a small increase of NO_x emission, justifying the lower level of soot at the exhaust with respect to the other strategies. This analysis was confirmed by NO measurements carried out in external combustion chamber.

Nanopulsed ultraviolet-visible absorption - extinction spectroscopy was applied in order to perform a quantitative analysis of OH, soot and NO in the optically accessible chamber [18, 19, 33].

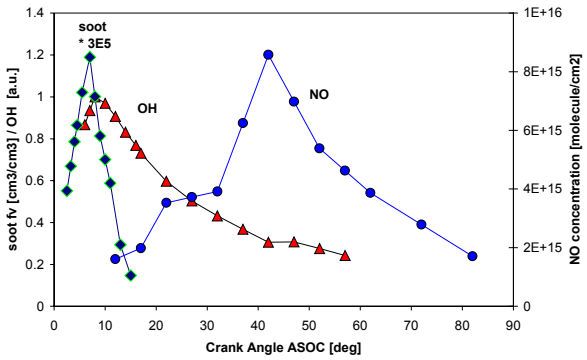

Figure 16. Soot volume fraction, OH radical concentration and NO concentration evaluated during main injection phase for the engine condition of Fig. 6.

The first absorption OH signal was observed during the fuel pyrolysis phase. In the same time, extinction measurements showed the first unstructured contribution, typical of soot particles precursors. [18] As it is reported in Figure 16, from 2°ASOC until 8° ASOC, OH absorption decreased correspond to the increasing of soot signals and heat release rate. In this time, the soot region expanded rapidly toward the chamber filling the entire volume in about 0.5 ms after start of combustion as observed both in the digital and spectral measurements carried out in all the chamber [33]. At 8°ASOC the soot decreased and new OH radicals were revealed. The OH radical produced in this phase could be considered as the marker of the soot oxidation. In fact, according to literature, the soot reduction was primarily a result of the attack of molecular oxygen and OH radicals [34].

The combination of extinction and scattering measurements allowed to retrieve the temporal evolution of soot particle size. Figure 17 reports mean diameters obtained for two locations of the combustion chamber downstream and upstream the zone of maximum liquid penetration, respectively. The upstream location was characterized by highest fuel/air ratio than the downstream one.

After the start of combustion, it is possible to a rapid increase of particle diameter, corresponding to the formation of carbonaceous soot precursors. In the upstream location, the increase of size is sharper than in the other one. In particular, the rapid increase is followed in a similar rapid decrease during the oxidation phase. In both locations, the oxidation phase is characterized by comparable value.

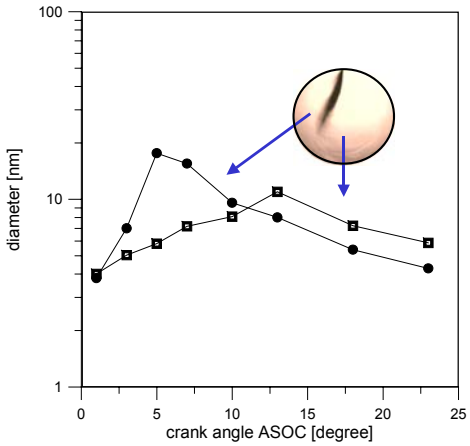

Figure 17. Time evolution of soot mean diameters measured in the chamber locations of picture.

These results were similar to those obtained for different fuel injections The size of soot particles results did not depend on fuel injection strategies. They influence the soot number density and thus mass concentration amount. Moreover, these results are comparable to those measured using a conventional injection system operating at low pressure [35]. In both cases, analogous spectral features were observed and soot diameters were smaller than 20 nm.

Another pollutant species detected in the combustion chamber is NO. Following in this analysis, the first signal of NO was observed during the soot oxidation phase, around 20° ASOC (Fig.16). Around 20° ASOC, OH radicals were consumed more quickly by NO formation [10, 36]. After 20° ASOC the post-oxidation phase occurred and NO concentration increased at decreasing OH concentration. NO concentration reached the highest value around 40° ASOC. After this time, a smooth NO decrease occurred due to the freezing of chemistry. NO formation times, observed in Figures 16, were shorter than those observed traditionally in diesel engines.

It had to be considered that the high degree of mixing, the high A/F ratios and the low charges induced a combustion process with a dominating premixed phase rather than a diffusive one. Such peculiarity yielded a more rapid NO formation than observed traditionally in transparent DI engines [8, 37]]. They worked in richer and more diffusive conditions. In any case, the NO formation times were in good agreement with those ones evaluated by other authors in similar combustion systems and measured with different techniques [38, 39].

Figure 18 shows the spatial distribution of NO absolute concentration, expressed in molecule/cm^2. Also in this case, spatial distributions are made of iso-contours built by spectral data detected in the measurement locations. Nitric oxide is expected to form in high temperature regions via the thermal NO mechanism. Formation rates are highest close to stoichiometric regions at the edge of the diffusion flame. Therefore, NO formation, like soot formation, is expected in the

diffusion flame zone, but at the lean side where more oxygen was present.

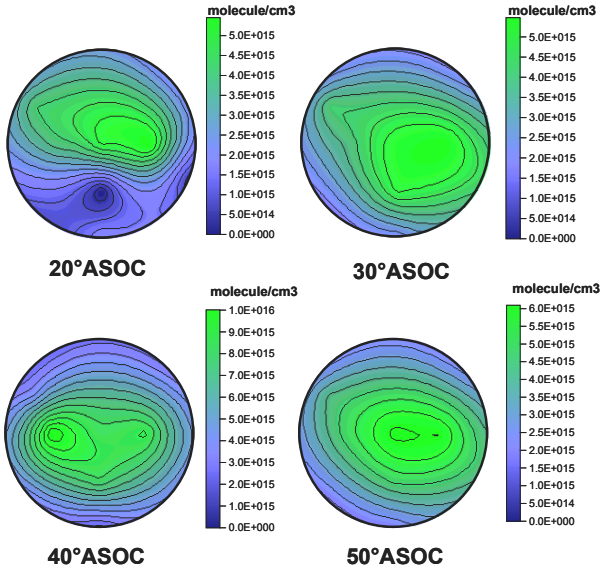

Figure 18. NO distribution evaluated during main injection phase for the engine condition of Fig. 6.

According to the Dec model, NO highest concentration should be just outside the soot region of the jet [11, 40]. These considerations are not valid in the case of this study, strongly influenced by the flow-field motion and geometry of the chamber. In particular, as reported in Figure 18, NO is distributed with homogeneity in a confined region in the centre of the chamber, due to the high turbulence induced by the swirl motion.
Moreover, the intake airflow produced a NO concentration gradient between the wall region and that along the axis of the tangential duct. It moved toward the principal combustion chamber and was induced by the expansion phase.

EXHAUST

The simultaneous application of multiwavelength extinction and scattering techniques allows characterising the diesel exhaust too. [20, 21]
Figure 19 reports the comparison between the particle size distribution evaluated at the exhaust of the engine with low pressure and high pressure (CR) injection system.. The first emitted high particulate mass and have a bimodal size distribution, characterised by nucleation and accumulation mode and not particularly sensible to change of load.
On the other side, in the clean condition, the size distribution shows an evolution from unimodal to a bimodal one at increasing loads.

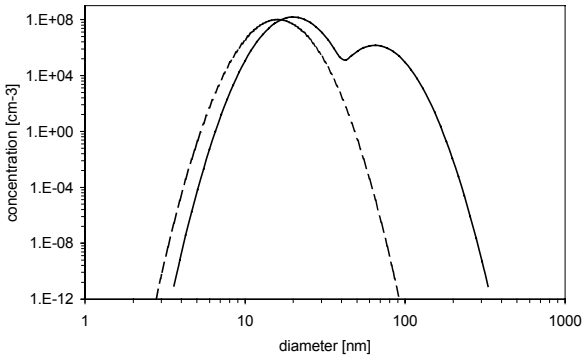

Figure 19. "High pressure" (dotted line) and "Low pressure" (full line) exhaust size distribution retrieved at same load and engine speed.

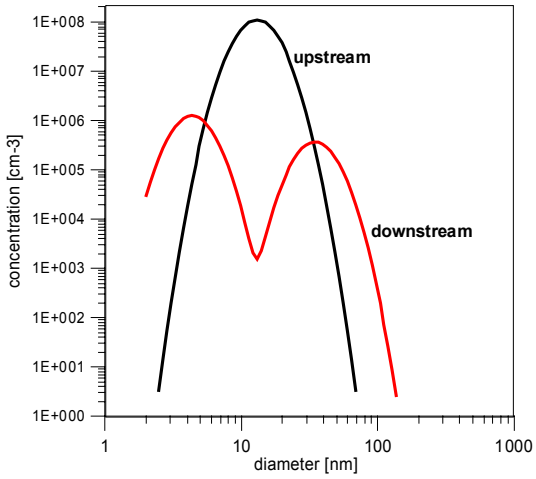

Figure 20. Exhaust size distribution evaluated upstream and downstream DPF at same load and engine speed.

Analogous analysis was carried out upstream and downstream DPF showed size distributions characterised by nucleation and accumulation mode with a mean size of 15 nm and 100 nm, respectively [23]. The first one was produced by the chemical interaction of soot organic precursors formed in the combustion chamber. The second class was the product of the surface growth, coagulation and coalescence of the first one. The relative number concentration of nucleation particles was more than three orders of magnitude greater than concentration of the accumulation mode. The increased concentration of nucleation particles was due to the formation of sulphate nanoparticles. These particles interacted with carbonaceous compounds and fragments due to the regeneration and produced mixing composition. The change in the size function distribution induced a global increase of mass and number of particles at the exhaust but not of the mean diameter.
These measurements did not only check the validity of the optical technique but also showed that the new diesel engine technologies, in spite of a drastic reduction of the exhaust particulate mass concentration, resulted in the emission in the

atmosphere of a high concentrations of carbonaceous nanoparticles.

CONCLUSION

Intensive research is in progress in the engine research laboratories of automotive companies and Universities in the world on engines, as we are approaching the introduction of more strict emission legislation, as the commitment to CO_2 reduction becomes imperative and the new fuel specifications come into play first in 2005 and then in 2010. This paper has presented a few examples of relevant research performed in the engine laboratories at Istituto Motori mainly on single-cylinder optical engines in combination with optical techniques. Although limited in scope, this paper focuses on topics, which are representative of on-going research in the automotive industry.

ACKNOWLEDGMENTS

Authors would like to acknowledge the contributions of their present and ex-students, and colleagues who co-authored the referenced papers.
Moreover, would like to thank Mr. Carlo Rossi and Mr. Bruno Sgammato for their precious help and technical support in the experimental activities.

REFERENCES

[1] Proceedings of THIESEL 2002 and Proceedings of THIESEL 2004. Int. Conference on Thermo and Fluid Dynamic Processes in Diesel Engines Valencia- Spain.

[2] Schommers J, Duvinage F, Stotz M, Peters A, Ellwanger S, Koyanagy K, and Gilden H (2000) Potential of Common Rail Injection System for Passenger Car DI Diesel Engines. SAE Paper n° 2000-01-0944.

[3] Bianchi G.M., Cazzoli G,. Pelloni P. and Corcione E.F (2002) Numerical Study Towards Smoke-Less And NOx-Less HSDI Diesel Engine Combustion. SAE Paper n° 2002-01-1115.

[4] Corcione E.F., Vaglieco B.M., Corcione,E.G., Lavorgna, M., Lanzafame R. (2003) - Study of the combustion of a new small DI Diesel Engine with Advanced Common Rail Injection System - JSAE/SAE Int. Spring Fuels & Lubricants,Yokohama (Japan) 2003, SAE Paper 2003-01-1782.

[5] Corcione E.F., Vaglieco B.M., Corcione, E.G., Lavorgna, M. (2002) - Potential of Multiple Injection Strategy for Low Emission Diesel Engines - SAE Paper 2002-01-1150, 2021-2027, vol. 111 SAE 2002 Trans Journal of Engines.

[6] Han, Z., Uludogan, A., Hampson, G.J and Reitz, R. D. (1996) - Mechanism and NOx Emissions Reduction Using Multiple Injection in a Diesel Engine - SAE Paper 960633.

[7] Pierpont, D. A., Montgomery, D.T., Reitz, R. D., (1994) Reducing Particulate and NOx Using Multiple Injections and EGR in a D.I. Diesel Engine. SAE Paper 940897.

[8] Zhao H and Ladommatos N. (2001). Engine Combustion Instrumentation and Diagnostics - 2001 SAE Int.

[9] Koyanagi K., Oing H., Renner G. and Maly R.R. (1999) - Optimizing Common Rail Injection by Optical Diagnostics in a Transparent Production Diesel Engines - SAE Paper n° 1999-01-3646.

[10] Heywood J.B. (1988) - Internal Combustion Engine Fundamentals - Mc Graw-Hill, NewYork.

[11] Dec J.E. (1997) -A Conceptual Model of D.I. Diesel Combustion Based on Laser Sheet Imaging. - SAE Paper n° 970873.

[12] Suzuki, M., Nishida, K. Hiroyasu, H. (1993) - Simultaneous Concentration Measurement of Vapor and Liquid in an Evaporating Diesel Spray - SAE Paper No. 930863

[13] Zhang. Y., Yoshizaki T., Nishida K. (2001). Quantitative Measurement of Droplets and Vapor Concentration Distributions in Diesel Sprays by Processing UV and Visible Images - SAE Paper: 2001-01-1294.

[14] Espey C. and Dec J. (1998) Chemiluminescence Imaging of Autoignition in A DI Diesel Engine. SAE Paper n° 982685.

[15] Merola S.S., Vaglieco B.M., Corcione E.F. and Mancaruso E. (2003) - In-cylinder Combustion Analysis by Flame Emission Spectroscopy of Transparent CR Diesel Engine. - SAE Paper n° 2003-01-1112.

[16] Merola S.S., Vaglieco B.M. and Mancaruso E. (2003) - Analysis of Combustion in a Transparent Common Rail Diesel Engine by 2D digital Imaging and Flame Emission Spectroscopy. - ASME Int. Congress ICES, Salzburg (AU) 17-19 May 2003, n° ICES 2003-01-644.

[17] Corcione E. F., Di Iorio S., Mancaruso E., Merola S. S., Vaglieco B. M. (2004)- Combustion Diagnostics of a Diesel Engine with Multiple Injection - THIESEL 2004 Conference on Thermo and Fluid Dynamic Processes in Diesel Engines Valencia- Spain, 7-10 September 2004.

[18] Merola S.S., Vaglieco B.M., D'Anna A., D'Alessio A. (2002) - Spectroscopic Analysis and Modeling of Particulate Formation In a Diesel Engine - JQRST 73, pp.443-450

[19] Merola S.S., Vaglieco B.M, Mancaruso E. (2004) - Multiwavelength Ultraviolet Absorption Spectroscopy of NO and OH Radical Concentration Applied to Diesel Engine - Experimental Thermal and Fluid Science 28 pp. 357-367.

[20] Merola S. S. and Vaglieco B. M. (2004) - Experimental and Modelling Characterisation of Nanometric Particles at the Exhaust of Common Rail Diesel Engine - Int. Journal on Energy for a Clean Environment vol.5, pp.1-14.

[21] Merola S.S., Vaglieco B.M., Zarinchang J. (2003) - Simultaneous Detection of NOx and Particulate in Exhaust of a CR Diesel Engine by UV-Visible Spectroscopy- SAE Paper n° 2003-01-0786 p. 2020-2029, vol. 112 SAE 2003 Trans Journal of Fuel.

[22] Bosch GmbH data sheet.

[23] Merola S.S., Vaglieco B.M. et al. (2004)-The Diesel Exhaust Aftertreatment (DEXA) Cluster: A Systematic Approach to Diesel Particulate Emission Control in Europe - SAE Paper n° 2004-01-0694.

[24] Gaydon AG, (1974) - The spectroscopy of flames - Chapman and Hall, London.

[25] Borghese, A.and Merola, S.S. (1998)– Time Resolved Spectral and Spatial Description of Laser-Induced Breakdown in Air as a Pulsed, Bright and Broadband Ultraviolet-Visible Light Source – Applied Optics, V.37 p, 3977-3083.

[26] Astarita M, Corcione E.F., Vaglieco B.M. and Valentino G (1999) - Optical Diagnostics of Temporal and Spatial Evolution of a Reacting Diesel Fuel Jet. - Comb. Sci. Tech, vol. 48,1-16.

[27] Merola S.S., Vaglieco B.M., Corcione E.F. and Formisano G. (2002)-Spectral Analysis of Combustion Process of Common Rail Diesel Engine. SAE Paper n° 2002-01-1634.

[28] Kerker, M. (1969)- The Scattering of Light and Other Electromagnetic Radiation - Academic Press, New York.

[29] Chang, H. and Charalampopoulos, T.T. (1990) - Determination of the wavelength dependence of refractive indices of flame soot - Proc.R.Soc. London A, 430, 577-591.

[30] Goldman A. and Gillis J. R. (1981).– Spectral Line Parameters for the A2Σ-X2Π (0,0) Band of OH for Atmospheric and High Temperatures – J. Quant. Spectrosc. Radiat. Transfer. V.25: 111-135.

[31]Okabe, I. (1978) - Photochemistry of small molecules – Wiley - Interscience Publications, J. Wiley & Sons ed., New York.

[32] Maunoury B, Duverger T, Mokaddem K and Lacas F (2002) Phenomenological Analysis of Injection, Autoignition and Combustion in a Small D. I. Diesel Engine SAE Paper n° 2002-01-1151.

[33] Merola S.S., Vaglieco B.M., Mancaruso E. (2003) - Soot Formation Analysis by Multiwavelength Spectroscopy in an External Chamber Diesel Engine equipped with a CR Injection System- SAE Paper n° 2003-01-1111.

[34] Nagle J., Strickland-Constable R. F. (1962)- Fifth Carbon Conference - vol. 1, p. 154, Pergamon, Oxford.

[35] Corcione E. F., Merola S.S., Vaglieco B. M. (2002) - Evaluation of Temporal and Spatial Distribution of Nanometric Particles in a Diesel Engine By Broadband Optical Techniques" Int. Journal of Engine Research, Vol.3-No2.

[36] Miller, J.A., Bowmann, C.T. (1985) - Mechanism and Modeling of Nitrogen Chemistry in Combustion - Prog. Energy Combust. Sci., 15, 287 – 338.

[37] Kidoguchi Y., Miwa K., Mohammadi A. (2001) - Reduction Mechanism of NOx in Rich and High Turbulence Diesel Combustion - The Fifth International Symposium on Diagnostic and Modeling of Combustion in Internal Combustion Engine, Comodia 2001, Nagoya, Japan, July 1-4, pp.108-114.

[38] Aoyagi, Y., Kamimoto, T., Matsui, Y., Matsuoka, S. (1980) - A Gas Sampling Study on the Formation Processes of Soot and NO in DI Diesel Engine - SAE Transaction, 89 (sec. 2), 1175 - 1189, paper n° 800254.

[39] Alatas, B., Pinson, J.A., Litzinger, T.A., Santavicca, D.A. (1993) - A Study of NO and Soot Evolution in a DI Diesel Engine via Planar Imaging - SAE Transactions, 102 (sec. 3), 1463 - 1473 paper n° 930973.

[40] Dec, J.E. and Cannan, R.E. (1998) - PLIF Imaging of NO Formation in a DI Diesel Engine - SAE, 79 - 105, paper n°980147.